

## Activity and Thermal Stability Improvements of Glucose Oxidase upon Adsorption on Core–Shell PMMA–BSA Nanoparticles

Chuanxin He,<sup>†,‡</sup> Jianhong Liu,<sup>\*,‡</sup> Laiyong Xie,<sup>†</sup> Qianling Zhang,<sup>‡</sup> Cuihua Li,<sup>‡</sup> Dayong Gui,<sup>‡</sup> Guangzhao Zhang,<sup>\*,†</sup> and Chi Wu<sup>†,§</sup>

<sup>†</sup>The Hefei National Laboratory for Physical Sciences at Microscale and Department of Chemical Physics, University of Science and Technology of China, Hefei, Anhui 230026, China, <sup>‡</sup>School of Chemistry and Chemical Engineering, Shenzhen University, Shenzhen, Guangdong 518060, China, and <sup>§</sup>Department of Chemistry, The Chinese University of Hong Kong, Shatin, N.T., Hong Kong

Received May 28, 2009. Revised Manuscript Received September 3, 2009

The interaction and adsorption of enzyme, glucose oxidase (GOx), on poly(methyl methacrylate)–bovine serum albumin (PMMA–BSA) particles were studied by using a quartz crystal microbalance with dissipation (QCM-D) and laser light scattering (LLS). The enzyme was irreversibly immobilized on the PMMA–BSA particle surface. The amount of enzyme immobilized on PMMA–BSA particles and the enzymatic activity were determined by UV/vis measurements. The influences of pH and ionic strength on the adsorption indicate that the electrostatic interaction plays a major role on the immobilization. The adsorbed GOx can retain at least 80% of the free enzyme activity. Thermal stability studies reveal that the adsorbed GOx only losses 28% of its activity in comparison with a 64% activity loss of free GOx when it is incubated at 50 °C for 35 h.

### Introduction

The development of biosensors, especially enzyme-based ones, has attracted much attention, which often involves the immobilization of proteins on some proper surfaces and conversion of chemical information into an electronic signal.<sup>1–5</sup> Different immobilization methods have been tried, including covalent

attachment,<sup>6–10</sup> physical entrapment or encapsulation,<sup>11–13</sup> and adsorption.<sup>14–24</sup> Covalent attachment often involves some complicated synthesis under some harsh experimental conditions, leading to a significant loss of enzymatic activity. Entrapment or encapsulation inside a solid matrix usually results in a low enzymatic reaction rate because substrates have to diffuse into the matrix to interact with the entrapped enzyme. In contrast, adsorption is a much simpler way to immobilize enzymes and maintain their activity under mild experimental conditions. However, the stability of adsorption is a problem, affected by a combination of factors, such as pH, ionic strength, temperature, surface tension, charges, and matrix. Therefore, a better understanding and control of the complicated protein adsorption on different surfaces is always needed for further development and improvement of various bioanalytical applications.

It is natural to use nanoparticles as a solid support to adsorb enzymes in the development of novel electrochemical biosensors with a fast electron transferring rate at the electrode surface because of its huge interfacial area. Much effort has been devoted to a combination of nanoparticles and protein immobilization.<sup>21,25–28</sup> Koutsopoulos et al.<sup>29</sup> showed that the adsorption of trypsin on hydrophobic (polystyrene) nanoparticles is stronger than that on a hydrophilic (silica) surface, but the amounts adsorbed on both of them at the adsorption equilibrium are similar. Caruso et al.<sup>30</sup> used a layer-by-layer self-assembly

\*To whom correspondence should be addressed

- (1) Caruso, F.; Rodda, E.; Furlong, D. N.; Niikura, K.; Okahata, Y. *Anal. Chem.* **1997**, *69*, 2043–2049.
- (2) Chen, X. H.; Hu, Y. B.; Wilson, G. S. *Biosens. Bioelectron.* **2002**, *17*, 1005–1013.
- (3) Muguruma, H.; Kase, Y.; Murata, N.; Matsumura, K. *J. Phys. Chem. B* **2006**, *110*, 26033–26039.
- (4) Wang, J. *Chem. Rev.* **2008**, *108*, 814–825.
- (5) Wang, J.; Liu, J.; Cepre, G. *Anal. Chem.* **1997**, *69*, 3124–3127.
- (6) Azioune, A.; Ben Slimane, A.; Ait Hamou, L.; Pleuvy, A.; Chehimi, M. M.; Perruchot, C.; Armes, S. P. *Langmuir* **2004**, *20*, 3350–3356.
- (7) Bousalem, S.; Mangeney, C.; Alcote, Y.; Chehimi, M. M.; Basinska, T.; Slomkowski, S. *Colloids Surf., A* **2004**, *249*, 91–94.
- (8) Pandey, P.; Singh, S. P.; Arya, S. K.; Gupta, V.; Datta, M.; Singh, S.; Malhotra, B. D. *Langmuir* **2007**, *23*, 3333–3337.
- (9) Patel, N.; Davies, M. C.; Hartshorne, M.; Heaton, R. J.; Roberts, C. J.; Tandler, S. J. B.; Williams, P. M. *Langmuir* **1997**, *13*, 6485–6490.
- (10) Saoudi, B.; Jammul, N.; Chehimi, M. M.; McCarthy, G. P.; Armes, S. P. *J. Colloid Interface Sci.* **1997**, *192*, 269–273.
- (11) Napoli, A.; Boerakker, M. J.; Tirelli, N.; Nolte, R. J. M.; Sommerdijk, N. A. J. M.; Hubbell, J. A. *Langmuir* **2004**, *20*, 3487–3491.
- (12) Zhu, H. G.; McShane, M. J. *Langmuir* **2005**, *21*, 424–430.
- (13) Zhu, H. G.; Srivastava, R.; Brown, J. Q.; McShane, M. J. *Bioconjugate Chem.* **2005**, *16*, 1451–1458.
- (14) Almeida, A. T.; Salvadori, M. C.; Petri, D. F. S. *Langmuir* **2002**, *18*, 6914–6920.
- (15) Anikin, K.; Röcker, C.; Wittemann, A.; Wiedenmann, J.; Ballauff, M.; Nienhaus, G. U. *J. Phys. Chem. B* **2005**, *109*, 5418–5420.
- (16) Fang, M.; Grant, P. S.; McShane, M. J.; Sukhorukov, G. B.; Golub, V. O.; Lvov, Y. M. *Langmuir* **2002**, *18*, 6338–6344.
- (17) Hibbert, D. B.; Gooding, J. J.; Erokhin, P. *Langmuir* **2002**, *18*, 1770–1776.
- (18) Karlsson, M.; Martensson, L.-G.; Jonsson, B.-H.; Carlsson, U. *Langmuir* **2000**, *16*, 8470–8479.
- (19) Koutsopoulos, S.; Tjeerdma, A.-M.; Lieshout, J. F. T.; van der Oost, J.; Norde, W. *Biomacromolecules* **2005**, *6*, 1176–1184.
- (20) Nguyen, T. H.; Elimelech, M. *Langmuir* **2007**, *23*, 3273–3279.
- (21) Palocci, C.; Chronopoulou, L.; Venditti, I.; Cernia, E.; Diociaiuti, M.; Fratoddi, I.; Russo, M. V. *Biomacromolecules* **2007**, *8*, 3047–3053.
- (22) Pescador, P.; Katakis, I.; Toca-Herrera, J. L.; Donath, E. *Langmuir* **2008**, *24*, 14108–14114.

- (23) Sigal, G. B.; Mrksich, M.; Whitesides, G. M. *J. Am. Chem. Soc.* **1998**, *120*, 3464–3473.
- (24) Vertegel, A. A.; Siegel, R. W.; Dordick, J. S. *Langmuir* **2004**, *20*, 6800–6807.
- (25) Azioune, A.; Pech, K.; Saoudi, B.; Chehimi, M. M.; McCarthy, G. P.; Armes, S. P. *Synth. Met.* **1999**, *102*, 1419–1420.
- (26) Brewer, S. H.; Glomm, W. R.; Johnson, M. C.; Knag, M. K.; Franzen, S. *Langmuir* **2005**, *21*, 9303–9307.
- (27) Duracher, D.; Elaissari, A.; Mallet, F.; Pichot, C. *Langmuir* **2000**, *16*, 9002–9008.
- (28) Nguyen, T. H.; Chen, K. L. *Environ. Sci. Technol.* **2007**, *41*, 5370–5375.
- (29) Koutsopoulos, S.; Patzsch, K.; Bosker, W. T. E.; Norde, W. *Langmuir* **2007**, *23*, 2000–2006.
- (30) Caruso, F.; Lichtenfeld, H.; Giersig, M.; Möhwald, H. *J. Am. Chem. Soc.* **1998**, *120*, 8523–8524.

approach to deposit charged proteins onto the surface of oppositely charged polystyrene nanoparticles. Most previous studies used particles made of synthetic polymer, inorganic, or metallic materials as substrates to adsorb proteins, which could severely limit their potential in vivo biomedical applications.<sup>31</sup>

Recently, we reported a method to prepare well-controlled poly(methyl methacrylate)–bovine serum albumin (PMMA–BSA) nanoparticles.<sup>32</sup> Transmission electron microscopy and X-ray photoelectron spectroscopy analysis confirms that they have an inert PMMA core and a biocompatible BSA protein shell. In the current study, we further used these biocompatible nanoparticles as a potential matrix to immobilize an enzyme, glucose oxidase (GOx), to maintain its activity. The adsorption of GOx on individual PMMA–BSA nanoparticles was studied by using a quartz crystal microbalance with dissipation (QCM-D), laser light scattering (LLS), and UV/vis adsorption. The activity and thermal stability of GOx adsorbed on PMMA–BSA surfaces were compared with those of GOx free in solution. The effects of pH and ionic strength on the adsorption were also studied to reveal the main driving force for the adsorption.

### Experimental Section

**Materials.** Bovine serum albumin (BSA), glucose oxidase (GOx from *Aspergillus niger*, 100 units/mg), and horseradish peroxidase (HRP, 250 units/mg) from Amresco were used as received.  $\beta$ -D-Glucose and *o*-dianisidine from Shanghai Sangon Biological Engineering Co. were used without further purification. Methyl methacrylate (MMA, from Shanghai Chemical Reagent) was first washed three times with a 5% sodium hydroxide solution to remove the inhibitor and then with deionized water until the pH in the water layer reached 7. The resultant MMA was further purified by distillation under vacuum before use. Copper chloride dihydrate, sodium chloride, potassium dihydrogen phosphate, and hydrochloric acid (also from Shanghai Chemical Reagent) were used as received without any purification.

**Preparation of PMMA–BSA Particles.** Spherical particles with a PMMA core and a BSA shell were prepared by using Cu<sup>2+</sup>-mediated graft copolymerization of methyl methacrylate directly from bovine serum albumin.<sup>32</sup> First, BSA was dissolved in deionized water at 25 °C in a water-jacketed flask equipped with a magnetic stirrer, a thermometer, a condenser, and a nitrogen inlet. The solution mixture was stirred for ca. 30 min before a designated amount of copper chloride aqueous solution was added. The solution mixture was purged with nitrogen for another 30 min prior to the addition of MMA. The polymerization was carried for 3 h with constant stirring under nitrogen. The resultant dispersion was purified by several cycles of centrifugation (11 000 rpm) and redispersion until no BSA and MMA were detectable in the supernatant. The dynamic laser light scattering measurement shows that such prepared particles are narrowly distributed with an average hydrodynamic radius ( $\langle R_h \rangle$ ) of 69 nm and a relative distribution width ( $\mu_2/\langle \Gamma^2 \rangle$ ) of 0.12.

**Adsorption and Desorption of GOx.** The adsorption of GOx on PMMA–BSA particles was performed in a polypropylene (PP) tube to avoid any possible adsorption of GOx on the tube wall. Each PP tube contained an identical concentration of PMMA–BSA particles but different amounts of GOx enzymes in a phosphate buffer (0.05 M and pH 4.5). The dispersions were incubated at room temperature. Our results showed that the adsorption of GOx on PMMA–BSA particles reaches a steady state after ca. 3 h. The particles adsorbed with GOx were separated from nonadsorbed GOx by centrifugation. The enzyme

concentrations before and after the adsorption were determined using the Bradford method with a calibration curve,<sup>33</sup> leading to the amount of GOx adsorbed onto PMMA–BSA. All the data points in each adsorption isotherm represent an average of three repeated measurements. The immobilization strength of GOx on PMMA–BSA was tested by redispersing and incubating these enzyme-covered particles in a phosphate buffer (0.05 M and pH 4.5) at room temperature for 24 h. The dispersion was centrifuged, and the GOx concentration in the supernatant was measured by UV adsorption at 280 nm.

**Enzymatic Activity of GOx.** The enzyme activity was determined by using the UV/vis adsorption method developed by Frederick et al.<sup>34</sup> The activities of GOx adsorbed on the particle surface and free in the dispersion were measured in a phosphate buffer. The specific activity of GOx free in the dispersion was taken as a reference, that is, 100%. In each measurement, 2.4 mL of *o*-dianisidine solution (0.2 mM), 0.3 mL of  $\beta$ -D-glucose solution (100 mg/mL), and 0.1 mL of HRP solution (~60 purpurogallin units/mL) were mixed in a cuvette in a phosphate buffer (0.05 M and pH 4.5). After the absorbance at 460 nm reached a constant, GOx was added to the solution mixture and the change of absorbance at 460 nm was recorded, resulting in a catalytic profile of GOx adsorbed on PMMA–BSA or free in solution mixture.

**Quartz Crystal Microbalance with Dissipation (QCM-D).** The QCM-D and AT-cut crystal with a fundamental resonant frequency of 5 MHz were from Q-sense AB. Detailed descriptions of the technique have been well documented.<sup>35–38</sup> Briefly, the mass of a thin layer on quartz crystal relates to the decrease in the resonant frequency of the crystal, whereas the dissipation factor is to the viscoelastic properties of the additional layer. The changes in the frequency and dissipation give information about the adsorption and structure of the adsorbed GOx. All the QCM-D experiments were conducted at 25 ± 0.02 °C.

**Laser Light Scattering (LLS).** A commercial LLS spectrometer (ALV/DLS/SLS-5022F) equipped with a multi- $\tau$  digital time correlation (ALV5000) and a cylindrical 22 mW UNIPHASE He–Ne laser ( $\lambda_0 = 632.8$  nm) as the light source was used. In dynamic LLS, the Laplace inversion of each measured intensity–intensity time correlation function [ $C^{(2)}(t, q)$ ] in the self-beating mode can result in a line-width distribution  $G(\Gamma, q)$ , where  $q$  is the scattering vector. For a pure diffusive relaxation,  $\Gamma$  is related to the translational diffusion coefficient  $D$  by  $\Gamma/q^2 = D$  at  $q \rightarrow 0$  and  $C \rightarrow 0$ , or a hydrodynamic radius  $R_h$  by  $R_h = k_B T / (6\pi\eta D)$  with  $k_B$ ,  $T$ , and  $\eta$  being the Boltzmann constant, absolute temperature, and solvent viscosity, respectively. Here, all the LLS measurements were done at  $\theta = 15^\circ$  and  $T = 25.0 \pm 0.1$  °C. Each solution or dispersion was clarified by using a 0.45  $\mu$ m Millipore PTFE filter to remove dust.

**Atomic Force Microscopy (AFM).** The AFM images were acquired on a multimode Digital Instruments apparatus with a tapping mode. The image of height was obtained by oscillating and scanning the cantilever horizontally on the plate at a given frequency, in which the oscillation amplitude or the height remains a constant but the substrate plate vertically moves. The vertical movement of the plate is converted to the asperity image of the substrate surface. The spring constant of the cantilever is in the range 20–100 N/m. The nominal radius of a new curvature tip is 5–10 nm. The cantilever length is 125  $\mu$ m with resonance frequency of 200–400 kHz. After each QCM study of the adsorption, the quartz crystal was taken out and dried in air

(33) Bradford, M. M. *Anal. Biochem.* **1976**, *72*, 248–254.

(34) Frederick, K. R.; Tung, J.; Emerick, R. S.; Masiarz, F. R.; Chamberlain, S. H.; Vasavada, A.; Rosenberg, S.; Chakraborty, S.; Schopfer, L. M.; Massey, V. *J. Biol. Chem.* **1990**, *265*, 3793–3802.

(35) Rodahl, M.; Höök, F.; Krozer, A.; Kasemo, B.; Breszinsky, P. *Rev. Sci. Instrum.* **1995**, *66*, 3924–3930.

(36) Sauerbrey, G. *Z. Phys.* **1959**, *155*, 206–222.

(37) Bottom, V. E. *Introduction to Quartz Crystal Unit Design*; van Nostrand Reinhold Co.: New York, 1982.

(38) Kanazawa, K. K.; Gordon, J. G. *Anal. Chem.* **1985**, *57*, 1770–1771.

(31) Wilson, G. S.; Hu, Y. B. *Chem. Rev.* **2000**, *100*, 2693–2704.

(32) He, C. X.; Liu, J. H.; Ye, X. D.; Xie, L. Y.; Zhang, Q. L.; Ren, X. Z.; Zhang, G. Z.; Wu, C. *Langmuir* **2008**, *24*, 10717–10722.

before the AFM measurements. In the current study, all the measurements were carried out at 25 °C. The data were analyzed with Nanoscope III software.

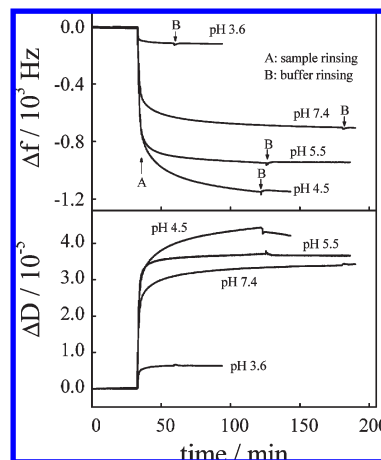
## Results and Discussion

Figure 1 shows the pH-dependence of the changes in the frequency and dissipation of the gold-coated quartz resonator after different PMMA–BSA dispersions are introduced. It is known that the frequency shift ( $\Delta f$ ) is attributed to the additional mass on the sensor surface, whereas the dissipation factor ( $\Delta D$ ) is related to the thickness and viscoelasticity of the adsorbed layer. Both  $\Delta f$  and  $\Delta D$  significantly change except at pH 3.6, indicating that PMMA–BSA particles are strongly adsorbed on the gold-coated quartz resonator. The repeated buffer washing has nearly no effect on either  $\Delta f$  or  $\Delta D$ , revealing that the adsorption is fairly strong and irreversible under these experimental conditions. The maximum adsorption occurs at pH 4.5, very close to the isoelectric point of PMMA–BSA (pH 5.1). Note that the  $\alpha$ -helix content of BSA changes more pronouncedly at pH 3.6 than at higher pH values,<sup>39</sup> presumably due to the entrapment of the only free cysteine on BSA inside so that it is not able to conjugate with the Au surface.<sup>40,41</sup> The strong electrostatic repulsion should also be responsible for the weak adsorption at pH 3.6.

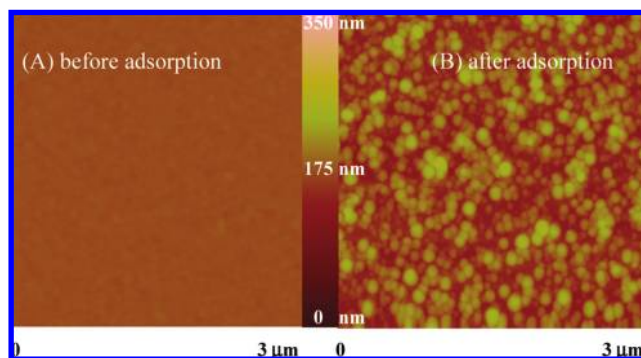
Figure 2 shows AFM images of the gold crystal surface before and after the adsorption of PMMA–BSA particles. As expected, the surface is fairly smooth with a root-mean-square (rms) roughness of  $\sim 1.8$  nm before the adsorption. The rms roughness increases to  $\sim 20.6$  nm after the adsorption, corresponding to  $\Delta f = 694$  Hz in QCM measurement. A combination of QCM and AFM studies shows that the gold crystal surface is fully covered by PMMA–BSA particles when  $\Delta f > 600$  Hz, which paved the way for our further study.

Figure 3 shows the adsorption of GOx on the PMMA–BSA-coated quartz crystal at different pH values, where the GOx concentration is maintained at 0.5 mg/mL. The frequency change ( $\Delta f$ ) is fairly small at pH 3.6, 5.5, and 7.4 after the buffer rinsing, indicating no adsorption of GOx on PMMA–BSA particles at these pH values. The GOx adsorption reaches a maximum at pH 4.5, where  $\Delta f = 124$  Hz after the buffer rinsing. It has been known that the protein adsorption is complicated, depending on many factors, such as the nature of substrate, protein, and solution composition. For the physical adsorption, the driving forces can include the van der Waals force, hydrogen bonding, and hydrophobic and electrostatic interaction.<sup>42–46</sup>

In the current study, the main driving force for the adsorption of GOx onto the BSA shell is a combination of electrostatic and hydrophobic interaction. Muguruma et al.<sup>3</sup> reported that GOx has a volume of  $6.0 \times 5.2 \times 7.7$  nm<sup>3</sup> and an isoelectric point (pI) of 4.2. We found that the pI of PMMA–BSA is  $\sim 5.1$ . Both PMMA–BSA and GOx are positively or negatively charged when the pH is  $< 4.2$  or  $> 5.1$  so that the electrostatic repulsion leads to no adsorption of GOx on PMMA–BSA. This explains why the maximum adsorption occurs at pH 4.5 just between the



**Figure 1.** pH-dependence of changes of frequency ( $\Delta f$ ) and dissipation ( $\Delta D$ ) after gold-coated quartz resonator is immersed in a PMMA–BSA dispersion ( $2.4 \times 10^{-4}$  g/mL), where the overtone number ( $n$ ) is 3.



**Figure 2.** AFM images of bare gold-coated crystal surface and PMMA–BSA particles adsorbed on gold-coated crystal surface at pH 4.5, where the quartz crystal was taken out after the QCM study and dried in air before AFM measurements.

pI values of PMMA–BSA and GOx, at which they are oppositely charged, as schematically shown in Figure 4.

On the other hand, the dynamic LLS study of the pH-dependent adsorption of GOx on PMMA–BSA shows that the average hydrodynamic radius ( $\langle R_h \rangle$ ) remains when GOx is added into the PMMA–BSA aqueous dispersion at either  $\text{pH} < 4.2$  or  $\text{pH} > 5.1$  but increases from  $\sim 69$  to  $\sim 85$  nm at pH 4.5, as shown in Figure 5. This agrees well with the QCM-D results. Further, Figure 6 shows how the ionic strength influences the adsorption of GOx on PMMA–BSA, where the GOx concentration is maintained at 0.5 mg/mL. As expected, the adsorption of GOx decreases as the ionic strength increases because  $\text{Na}^+$  and  $\text{Cl}^-$  ions screen out the electrostatic attraction between oppositely charged GOx and PMMA–BSA. Therefore, we are able to conclude that the electrostatic attraction between positively charged PMMA–BSA and negatively charged GOx is the primary driving force for the adsorption.

Figure 7 shows the adsorption isotherm of GOx onto PMMA–BSA at 25 °C, where  $\text{GOx}_{\text{adsorbed}}$  and  $C_{\text{GOx}}$  are, respectively, the maximum amount of enzyme adsorbed per unit mass and the final enzyme concentration. Each data point in Figure 7 represents an average of three repeated measurements. The adsorption isotherm displays two regions. In the low enzyme concentration range (0.05–0.18 mg/mL), the adsorption increases rapidly with the increase of GOx concentration because of the strong electrostatic attraction between the negatively charged GOx and the

(39) Belegriou, S.; Mannelli, I.; Lisboa, P.; Bretagnol, F.; Valsesia, A.; Ceccone, G.; Colpo, P.; Rauscher, H.; Rossi, F. *Langmuir* **2008**, *24*, 7251–7261.

(40) Bontempo, D.; Heredia, K. L.; Fish, B. A.; Maynard, H. D. *J. Am. Chem. Soc.* **2004**, *126*, 15372–15373.

(41) Heredia, K. L.; Bontempo, D.; Ly, T.; Byers, J. T.; Halstenberg, S.; Maynard, H. D. *J. Am. Chem. Soc.* **2005**, *127*, 16955–16960.

(42) Arai, T.; Norde, W. *Colloids Surf.* **1990**, *51*, 1–15.

(43) Azioune, A.; Chehimi, M. M.; Miksa, B.; Basinska, T.; Slomkowski, S. *Langmuir* **2002**, *18*, 1150–1156.

(44) Haynes, C. A.; Norde, W. *Colloids Surf., B* **1994**, *2*, 517–566.

(45) Jackson, D. R.; Omanovic, S.; Roscoe, S. G. *Langmuir* **2000**, *16*, 5449–5457.

(46) Ostuni, E.; Grzybowski, B. A.; Mrksich, M.; Roberts, C. S.; Whitesides, G. M. *Langmuir* **2003**, *19*, 1861–1872.

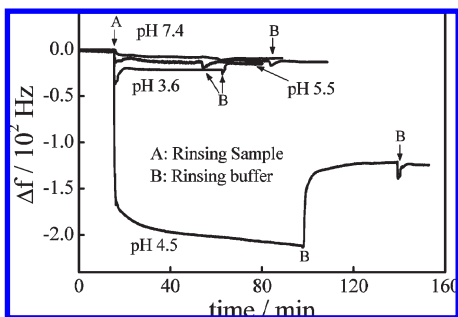


**Figure 3.** Time-dependence of GOx adsorbed on PMMA-BSA at different pH values, where  $C_{GOx} = 0.5$  mg/mL.

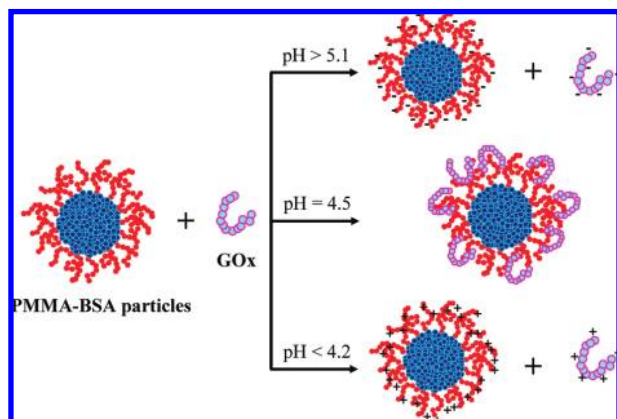


**Figure 4.** Schematic of GOx adsorbed on spherical PMMA-BSA particles in aqueous solutions with different pH values.

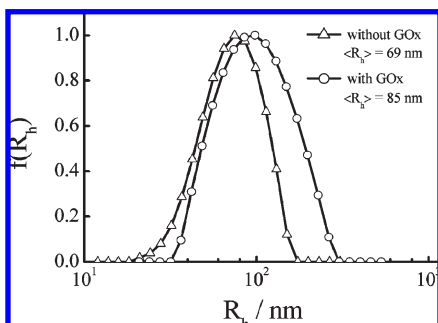


**Figure 5.** Hydrodynamic radius distributions  $f(R_h)$  of PMMA-BSA particles before and after they are mixed with GOx in a 0.05 M phosphate buffer (pH 4.5), where  $C_{BSA-PMMA} = 3.1 \times 10^{-5}$  g/mL and  $C_{GOx} = 1.7 \times 10^{-5}$  g/mL.

positively charged PMMA-BSA particles at pH 4.5. Further increasing the GOx concentration leads the charges on the nanoparticle surface to be screened out, so that the adsorption reaches a plateau at higher GOx concentration.

For the physical adsorption, it is always a challenge to prevent or reduce the desorption of enzyme in applications, especially for useful biosensors. In the current study, the desorption of enzyme was tested by redispersing the GOx-covered particles in the original buffer. We found no detectable GOx enzyme in the supernatant after incubating the dispersion overnight. Furthermore, we found that heating the dispersion to 50 °C for 6 h also induces no desorption of GOx from PMMA-BSA. Such thermal stability is important for the enzymatic activity test. Presumably, each enzyme molecule is anchored on the PMMA-BSA surface via multiple adsorption points besides hydrogen bonding between

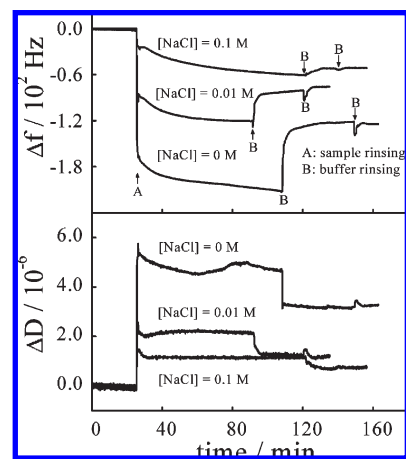


**Figure 6.** NaCl concentration dependence of changes in frequency ( $\Delta f$ ) and dissipation ( $\Delta D$ ) after GOx enzymes are adsorbed on PMMA-BSA at pH 4.5, where  $C_{GOx} = 0.5$  mg/mL.

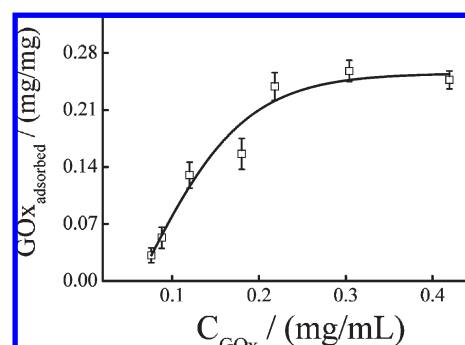


**Figure 7.** Adsorption isotherm of GOx enzyme on PMMA-BSA particles in a phosphate buffer (0.05 M and pH 4.5), where  $GOx_{adsorbed}$  is the maximum adsorption at 25 °C.

GOx and BSA, resulting in the observed irreversible adsorption. The clustering of those adsorbed GOx molecules on PMMA-BSA might also be responsible for the low desorption because it is more difficult to detach a cluster of many protein chains than individual GOx molecules.

The enzymatic activity difference between GOx free in the dispersion and adsorbed on PMMA-BSA was measured in a phosphate buffer, where the Bradford method was used to determine the protein content<sup>33</sup> and the specific activity of GOx free in the dispersion was used as a reference point (100%). Figure 8 shows a comparison of catalytic activities of free and adsorbed GOx molecules. The absorbance at 460 nm linearly increases with time before reaching a plateau. The slope of the linear increment part of each curve is used to compare the relative activity of free and adsorbed GOx molecules. The calculation shows that adsorbed GOx preserves ~84% of the total activity per unit mass in comparison with free GOx. The slight decrease of the total enzyme activity might be attributed to the conformational change of some GOx molecules after the adsorption.<sup>44</sup> Our results also reveal that the adsorbed GOx has a higher catalytic activity at pH 7.4, close to the physiological environment, in comparison with that at pH 4.5. The apparent Michaelis-Menten constant,<sup>47</sup> a characteristic of the enzyme reaction kinetics, was estimated to be ~20 mM, close to that of free GOx in solution (18 mM). Therefore, the adsorption of GOx on PMMA-BSA particles can retain its activity and lead to a higher affinity to glucose because of

(47) Blandino, A.; Macias, M.; Cantero, D. *Process Biochem.* **2001**, *36*, 601–606.

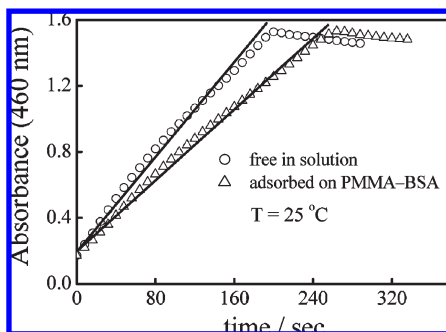


**Figure 8.** Time-dependence of enzyme activity of GOx before and after it is adsorbed on PMMA-BSA in a 0.05 M phosphate buffer (pH 4.5).

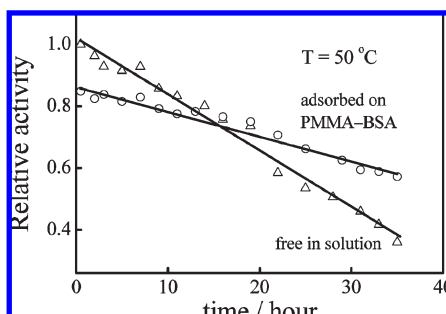


**Figure 9.** Time-dependent thermal stability of GOx before and after it is adsorbed on PMMA-BSA in a 0.05 M phosphate buffer (pH 4.5).

a mild immobilization condition and the biocompatible surface of PMMA-BSA particles. We will further use these particles as a matrix to immobilize GOx to develop high performance glucose biosensors in the future.

The stability of GOx depends on both temperature and standing time. It has been reported that GOx free in a solution

incubated at room temperature started to lose its activity only after  $\sim 4$  days, but loses 90% of its activity if the solution was heated at 60 °C for  $\sim 3$  h.<sup>5,11</sup> We studied the effect of heating on the stability of GOx at 50 °C. Figure 9 shows that the thermal stability of GOx adsorbed on PMMA-BSA is much better than that of GOx free in the dispersion. The adsorbed and free GOx lost 28% and 64% of its activity, respectively, when they were incubated at 50 °C for 35 h. The adsorbed GOx still retains 84% of its activity even at 50 °C for 10 h, indicating that the substrate accessibility is slightly affected when the solution is heated up to 50 °C. The better thermal stability is presumably attributed to the fact that the immobilization of GOx on PMMA-BSA stabilizes the protein structure.

## Conclusion

Glucose oxidase (GOx) strongly adsorbs on spherical PMMA-BSA core-shell nanoparticles at pH  $\sim 4.5$ , just between the pI values of GOx and PMMA-BSA particles, revealing that the main driving force is the electrostatic attraction between oppositely charged GOx and PMMA-BSA at this pH. The adsorption of GOx under a mild experimental condition can minimize a possible change of the enzyme conformation and preserve at least 80% of its activity in comparison with GOx free in the dispersion. The immobilization of GOx on biocompatible PMMA-BSA particles can also significantly improve its thermal stability. Our current results demonstrate that PMMA-BSA particles with a biocompatible BSA shell as a promising substrate provide a platform to immobilize other enzymes or proteins, for different potential applications, especially for the development of novel biosensors.

**Acknowledgment.** The financial support of the Ministry of Science and Technology of China (2007CB936401), the National Natural Scientific Foundation of China (NNSFC) Projects (20601019, 50773077, and 50333050), and the Hong Kong Special Administration Region (HKSAR) Earmarked Project (CUHK4037/06P, 2160298) is gratefully acknowledged.